Maritime Engineering
Volume 168 Issue MA2
Slope failure by unstable breaching
van Rhee

ice | proceedings

Proceedings of the Institution of Civil Engineers
Maritime Engineering 168 June 2015 Issue MA2
Pages 84–92 http://dx.doi.org/10.1680/maen.14.00006
Paper 2014-6
Received 01/04/2014 Accepted 12/02/2015
Keywords: dredging/failures/hyraulics & hydromechanics

ice Institution of Civil Engineers
publishing

Slope failure by unstable breaching

Cees van Rhee
Professor, Delft University of Technology, Faculty of Mechanical, Maritime and Materials Engineering, Section of Dredging Engineering, Delft University of Technology, Delft, the Netherlands

During the last decades, the breaching process as a production mechanism for stationary suction dredgers has become less important and therefore little research has been directed towards this process. It was not very well known as a cause of slope failures outside the dredging community until some years ago, but is now more accepted as a failure mechanism in the geotechnical world. In this paper the unstable breaching mechanism is explained. The breaching process is simulated using a two-dimensional computational fluid dynamics code with a special boundary condition at the bed. This leads to a better understanding of the process and how unstable situations can be predicted.

Notation

A	constant
a	hindered settling coefficient
C_v	consolidation coefficient (m^2/s)
$\bar{c}$	total concentration
$\bar{c}_b$	total near bed concentration
$D*$	dimensionless particle diameter
D_{50}	mean particle size (m)
E	pick-up flux (kgm^2/s)
F	constant
$\boldsymbol{g}$	accelleration due to gravity
H	height of the active wall (m)
i_{crit}	critical slope angle
i_{eq}	equilibrium slope angle
k_0	in-situ permeability (m/s)
k_l	permeability at the loose state (m/s)
k_s	roughness height according to Nikuradse (m)
N	number of fractions
$\vec{n}$	normal vector
n	porosity
n_0	in situ porosity
n_{crit}	critical porosity
n_{min}	minimum porosity
n_{max}	maximum porosity
n_1	porosity at a looses state
p	pressure (Pa)
$R_c=(1-n_0-\ c_b)/(1-n_0)$	reduction factor due to near bed concentration
R_α	reduction factor due to slope angle
S	sedimentation flux ($kg/m^2/s$)
s	sediment flux (kg/m/s)
u	horizontal flow velocity (m/s)
u_*	friction velocity (m/s)
$us=\sqrt{\vec{g}\Delta D50}$	definition (m/s)
$\vec{v}$	velocity (m/s)
v_e	erosion velocity (m/s)
v_s	slip velocity (m/s)
v_{sed}	sedimentation velocity (m/s)
v_w	active wall velocity (m/s)
v_z	vertical velocity of a particle (m/s)
w	vertical flow velocity (m/s)
Y	distance to the wall (m)
α	slope angle (rad)
β_{eq}	equilibrium slope angle $i_{eq}=\tan\beta_{eq}$ (rad)
Γ	diffusion coefficient (m^2/s)
$\Delta=(\rho_s-\rho_w)/\rho_w$	specific density
Δn	relative porosity change
θ	shields parameter
θ_0	shields parameter
θ_{cr}	critical Shields parameter
κ	von Kármàn constant
μ	dynamic viscosity (kg/m/s)
μ_Y	velocity in the gridpoint close to the wall (m/s)
ν	kinematic viscosity (m^2/s)
ν_e	eddy viscosity (m^2/s)
ρ	mixture density (kg/m^3)
ρ_s	density of particles (kg/m^3)
ρ_w	density of water (kg/m^3)
σ	Schmidt–Prandtl number
τ	shear stress (N/m^2)
τ_b	bed shear stress (N/m^2)
$\Phi_p=E/(\rho_s u_s)$	dimensionless pick-up
ϕ	internal friction angle (rad)

1. Introduction

Stability of (submarine) slopes is a classic problem in soil mechanics. The most frequently encountered failure mechanism is (rotational) sliding of the soil mass owing to gravity. Submarine slopes are normally saturated and under these conditions static liquefaction can be responsible for their failure. Static liquefaction is mostly encountered in loose sands that show contraction under shear. A large part of the soil body loses strength and can flow away as a very dense fluid. Owing to the presence of silt, a low value of permeability will increase the susceptibility for liquefaction as excess pressure will be more persistent.

A less known failure mechanism is breaching. Unlike static liquefaction, this mechanism can occur in very dense sands. The breaching process is a very important production mechanism for stationary suction dredgers. By insertion of a suction mouth in a sand layer, a steep underwater slope is created. The disturbance of the slope progresses slowly in a radial direction. The sand particles flow to the deepest part of the pit where the suction mouth is positioned.

Figure 1 shows the breaching process on a laboratory scale. At the toe of a slope a suction tube is inserted in the sand body. Sand is sucked into the tube and a steep slope travels in a radial direction. The lines show the position of the slope in time. The labels indicate the time in seconds after the insertion of the tube. The process in Figure 1 is typically encountered in small-scale laboratory tests. The slope angle below the sand producing part of the slope is close to the natural angle of repose of the slope. The steep part (where the slope angle is larger than the angle of repose) of the slope is called the active wall. In dredging practice the height of the active wall is often much higher than when performed at a laboratory scale (up to 5 m is not uncommon (Vlasblom, 2003)). In that case the sand will flow to the deepest part of the pit as a turbulent density current and much gentler slopes will develop with angles smaller than the natural angle of repose (Koning, 1970). The breaching process can also be responsible for unwanted slope instability during underwater slope construction, as will be discussed in the next section.

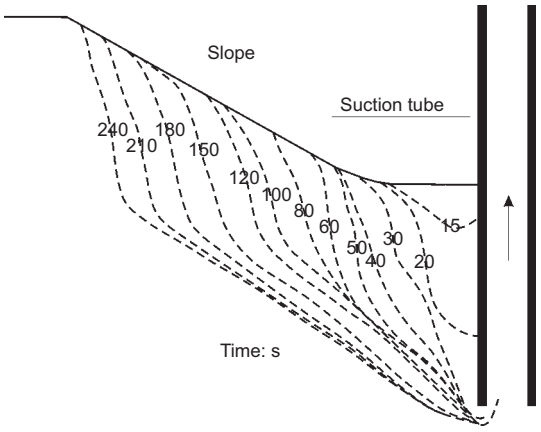

Figure 1. Breaching process on a laboratory scale (Breusers, 1974)

2. Stable and unstable breaching

In the 1980s breaching experiments were carried in the dredging flume of Deltares with sand layers of about 2 m high. The scale of these experiments was large enough to create turbulent sand–water density currents on the slope and the effect of erosion owing to these currents was measured. Around the same time, large-scale tests were carried out to investigate the development of underwater slopes during sand fill operations (Mastbergen and Winterwerp, 1988). These tests demonstrate that slope angles of the created sand bodies decreased with increasing sand production. The shallow slope angles and erosion due to the density current can lead to an unstable breaching process. A breaching process is referred to as being unstable when a certain disturbance on a slope (local steepening) will not gradually diminish, but will increase in size, which can lead to an uncontrolled retrogressive failure of a slope (Figure 2). This mechanism was first reported by van Rhee and Bezuijen (1998), but it is very likely that this mechanism was also responsible for slope failures of densely packed banks of the Mississippi River (Torrey, 1995). Later this mechanism was recognised by others (Groot *et al.*, 2009; Mastbergen and van den Berg, 2003).

The stable or unstable breaching mechanism is presented in Figure 3. The figure shows two different situations on a slope. Both figures show a slope with a local steep part after removal

Figure 2. Damaged lake border after unstable breaching (Groot *et al.*, 2009)

of a volume of sand at the toe. In both situations the disturbance will travel to the left, but in Figure 3(a) the local steepening will gradually diminish, whereas in Figure 3(b) the height of the local instability will increase in size. The latter is called an unstable breaching process.

Often the unstable breaching process is confused with static liquefaction. The failure mechanisms are, however, totally different. Static liquefaction is mostly encountered in loose sands, which show contraction under shear (although dilative soils also tend to show a little contraction directly after application of a load, which may be sufficient for the initiation of liquefaction (de Jager *et al.*, 2008)). Nevertheless, contraction is needed to generate excess pore pressure and consequently decrease in effective stress. A large part of the soil body loses strength and can flow away as a very dense fluid. A low value of permeability, due to the presence of silt, will increase the susceptibility for liquefaction as excess pore pressure will be more persistent. Unstable breaching can take place in very dense sands. The slope is internally stable owing to negative excess pore pressure (Meijer and van Os, 1976; van Rhee and Bezuijen, 1998; You *et al.*, 2012). Failure takes place at the surface owing to a hydraulic process (erosion by a density current), apart from the upper side of the active wall where particles drop off the surface owing to gravity and where small slides are observed. A lower value of permeability due to the presence of silt will decrease susceptibility for unstable breaching because the production of the active wall increases with permeability, as will be shown in the next section. Another difference between the two failure mechanisms is the time scale. It can take several hours (depending on the slope geometry) before the unstable breaching process comes to an end, whereas the time scale of static liquefaction is probably a matter of minutes. The resulting slope profiles after failure are nevertheless often very similar. It is also possible that static liquefaction acts as a trigger for unstable breaching. After liquefaction the slope is steepened locally and this disturbance will proceed as an unstable breach.

2.1 Analytical approach

Whether the development of a local disturbance is stable or unstable depends on the sand characteristics, the initial breach height and the initial slope angle. In van Rhee and Bezuijen (1998) a simple stability condition was derived. The process is stable when the sand mass flowing from local disturbance (active wall) tends to settle at a steeper angle compared with the slope angle below this active wall, as can be seen in Figure 3(a). Hence the stability is related to the deposition slope angle and the sand flux flowing from the active wall. In Mastbergen and Winterwerp (1988) large-scale tests were carried out to investigate the development of underwater slopes during sand fill operations. The equilibrium slope angles were measured and the following empirical relationship was obtained

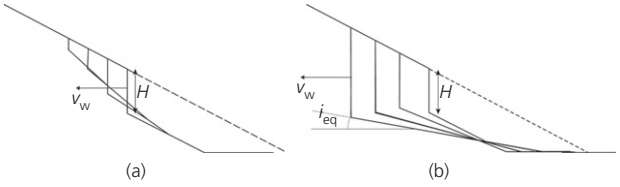

Figure 3. Schematic illustration of different breaching modes: (a) stable breaching; (b) unstable breaching

$$1. \quad i_{eq} = 0{\cdot}0049 s^{-0{\cdot}39} D_{50}^{0{\cdot}92}$$

where $i_{eq} = \tan \beta_{eq}$, β_{eq} is equilibrium slope angle, s is sediment flux and D_{50} is mean particle size. Note that the dimension of D_{50} is micrometres (μm) in this equation. When a sand–water mixture is flowing over a slope and the slope angle is gentler than the equilibrium slope angle, according to Equation 1 the sand particles will settle on the slope. If the slope angle is steeper compared with the equilibrium slope, the mixture will erode the slope. The sand flux flowing from the active wall follows from continuity and reads

$$2. \quad s = \rho_s (1 - n_0) H v_w$$

where ρ_s is density of the particles, n_0 is porosity of the sand body, H is height of the active wall and v_w is horizontal velocity of the active wall. The active wall velocity is (van Rhee, 2010)

$$3. \quad v_w = (1 - n_0) \frac{\rho_s - \rho_w}{\rho_w} \frac{k_1}{\Delta n} \cdot \cot \phi$$

where ρ_w is density of water, k_1 is permeability at the loose state and ϕ is internal friction angle and Δn is relative change in porosity. The relative porosity change is defined as

$$4. \quad \Delta n = \frac{n_1 - n_0}{1 - n_1}$$

The value of n_1 and corresponding permeability k_1 are, however, not easy to determine. It is assumed that

$$5. \quad (1 - n_0) \frac{k_1}{\Delta n} = F k_0$$

where F is assumed to be a constant. The permeability depends on the porosity. In general the following relation is found in the literature

$$6. \quad k = f(D_{15}) \frac{n^3}{(1 - n)^2}$$

where $f(D_{15})$ is a function of the particle size and n the porosity. In that case F reads

$$7. \quad F = \frac{(1-n_0)}{\Delta n}\frac{k_1}{k_0} = \frac{n_l^3}{n_0^3}\frac{(1-n_0)^3}{(n_1-n_0)(1-n_1)}$$

Typical values for the porosities are $n_{min} = 0{\cdot}35$, $n_{crit} = 0{\cdot}44$ and $n_1 = n_{max} = 0{\cdot}48$. For dense sands n_0 will vary between n_{min} and n_{crit}. When it is assumed that $n_1 = n_{max}$ the value of F varies between 9 and 10. For typical values of $\rho_s = 2650\ \text{kg/m}^3$, $\rho_w = 1000\ \text{kg/m}^3$ and $\phi = 30°$, the equation for the active wall can be simplified to

$$8. \quad v_w = 10\frac{\rho_s - \rho_w}{\rho_w}\cot\phi\ k_0 = 10 \times 1{\cdot}65 \times 1{\cdot}73 k_0 = 28k_0$$

This agrees with model tests where it appeared that $20k_0 < v_w < 40k_0$ (Breusers, 1977), and this also agrees with the findings of (You *et al.*, 2012) where the following expression was obtained

$$9. \quad v_w = \delta\eta C_v$$

where δ is a function of compressibility E. The consolidation coefficient $C_v = \frac{k}{\mu E}$ and μ is the dynamic viscosity. The factor η takes into account that the principal stress ratio and hence water under pressure decays with distance from the active wall. The values for δ and η are difficult to obtain, hence the practical value of Equation 9 is limited. In You *et al.* (2012) small-scale experiments were carried out on silty sand with a $D_{50} = 140$ μm. The permeability of the sand was measured using a falling head test ($k_0 = 4 \times 10^{-5}$ m/s). The expected active wall velocity for these experiments would vary between $(20-40)k_0$ or 0·8–1·6 mm/s. The active wall velocity in the tests can be derived from the pore pressure measurements (which can be found in the repository referenced in You *et al.* (2012)) and varied between 0·7 and 1·3 mm/s. This falls within the expected range.

Combining the expression for the active wall velocity, Equation 2, Equation 1 and $v_w = 30k_0$ yields the following expression for the critical slope angle

$$10. \quad i_{crit} = 0{\cdot}0049[30\rho_s(1-n_0)Hk_0]^{-0{\cdot}39} D_{50}^{0{\cdot}92}$$

When the slope angle below an active wall with height H is gentler than i_{crit} the active wall height will decrease, hence the breach is stable. Figure 4 shows a contour plot of the critical slope angle in degrees as a function of particle size D_{50} and active wall height H (hence the labels in the lines show the critical angle in degrees). The permeability is not directly related to D_{50}, but more to D_{15}. The equation of den Adel is used to calculate permeability (den Adel, 1987; van Rhee, 2010).

$$11. \quad k_0 = \frac{\boldsymbol{g}}{160\nu} D_{15}^2 \frac{n_0^3}{(1-n_0)^2}$$

where ν is kinematic viscosity.

For the figure the ratio between $D_{50}/D_{15} = 1{\cdot}35$ is kept constant in order to determine a value for the permeability as a function of D_{50}. The figure shows that for a small active wall height the critical slope angle is close to the angle of repose. For higher values the critical slope angle is reduced by the effect of the turbulent density current.

3. Numerical simulation of breaching process

3.1 Introduction

It was shown above that the influence of the turbulent density current flowing over the slope determines the stability of the breaching process. Using a computational fluid dynamics model the stability was investigated more in detail. The model used was based on the two-dimensional (2DV) model originally developed to simulate the hopper sedimentation process. For detailed information refer to van Rhee (2002). The 2DV model is based on the Reynolds averaged Navier–Stokes equations (RANS). The model is hydrodynamic (non-hydrostatic) and a mixture flow approach (drift–flux model) is used. The density in the momentum equations is the mixture density, hence the sediment water mixture is regarded as a fluid. The density can change in time and space depending on the local sediment concentration. The mixture model is an alternative for a multi-phase approach where the momentum equation is solved for every phase. This leads to a large number of equations when the influence of the particle size distribution is to be included. The interaction between the different phases is difficult to model and the simulations are time consuming and often unstable. Originally the model was only capable of simulating flows where only sedimentation occurred. The model will be extended below to simulate eroding flows.

3.2 Governing equations

The horizontal and vertical momentum equation applied on a control volume $d\Omega$ with surface area dS reads

$$12. \quad \begin{aligned} \frac{\partial}{\partial t}\int_\Omega \rho u \mathrm{d}\Omega + \int_S \rho u\vec{v}\,.\,\vec{n}\mathrm{d}S &= \int_S \tau_{xj}\vec{i}_j\,.\,\vec{n}\mathrm{d}S - \int_S p\vec{i}_x\,.\,\vec{n}\mathrm{d}S \\ \frac{\partial}{\partial t}\int_\Omega \rho w \mathrm{d}\Omega + \int_S \rho w\vec{v}\,.\,\vec{n}\mathrm{d}S &= \int_S \tau_{zj}\vec{i}_j\,.\,\vec{n}\mathrm{d}S - \int_S p\vec{i}_z\,.\,\vec{n}\mathrm{d}S - \int_\Omega \rho\vec{g}\mathrm{d}\Omega \end{aligned}$$

where u is horizontal flow velocity, w is vertical flow velocity, $\vec{v}$ is velocity vector, p is pressure, ρ is density of the sediment

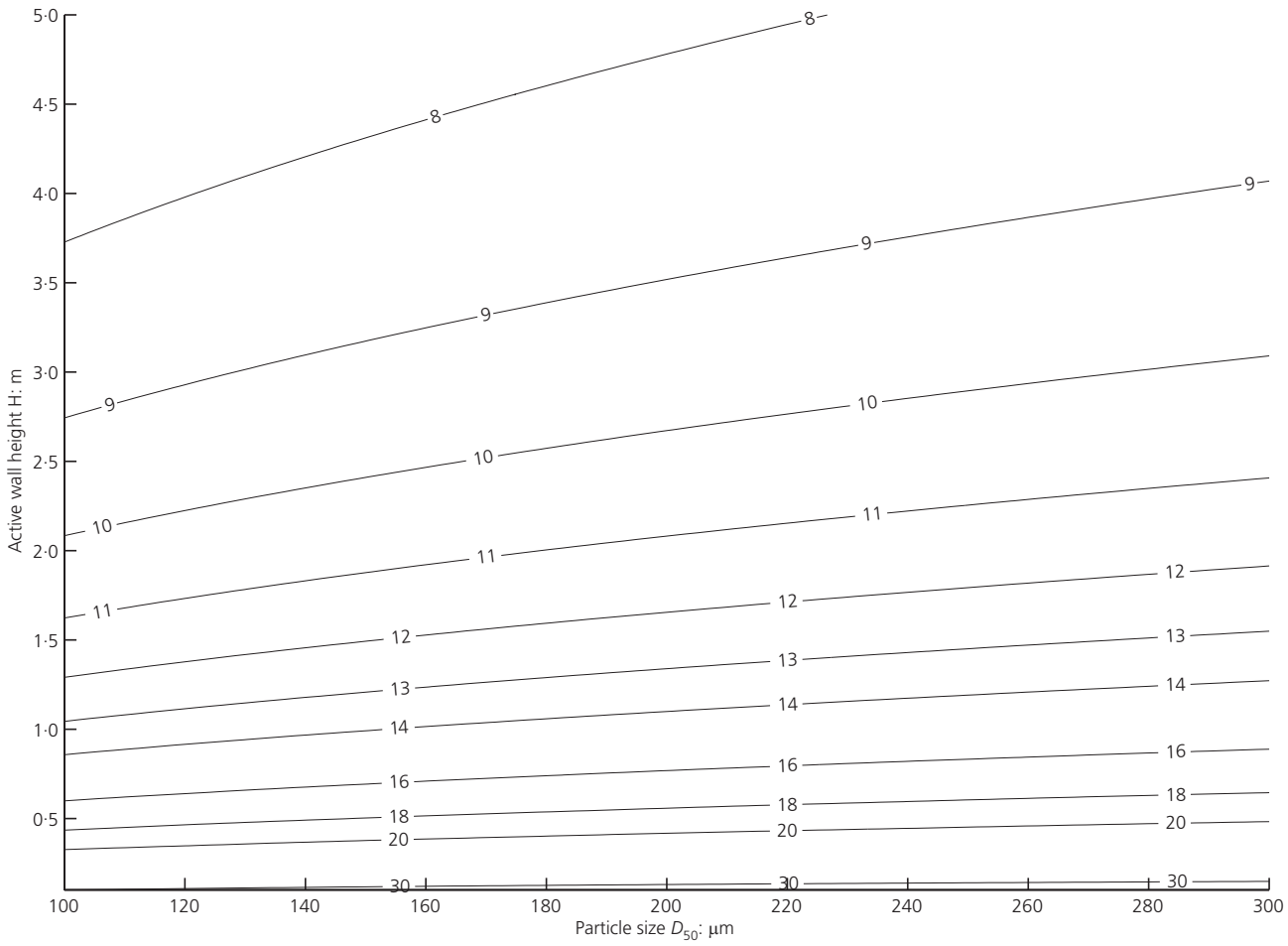

Figure 4. Critical slope angle i_{crit} (degrees)

water mixture, τ is shear stress, $\vec{i}_x$, $\vec{i}_z$ are unity vectors in x and z direction, respectively, and $\vec{n}$ is normal vector.

The continuity equation for incompressible flows in conservative notation reads

$$13. \quad \int_S \vec{v} \,.\, \vec{n} \mathrm{d}S = 0$$

The equations are Reynolds averaged and turbulent closure is obtained using the standard $k-\varepsilon$ model (with standard values for the coefficients).

3.3 Sediment transport

The model was originally developed for hopper sedimentation, where high sediment concentrations occur, and suspended sediment transport dominates over bed load transport. Bed load transport is therefore neglected in the model. The particle size distribution is approximated with a finite number N of different particle diameters. The concentration of a certain fraction with grain diameter D_k is c_k. The mixture density ρ as present in the momentum (Equation 12) is computed using the concentration of the different fractions

$$14. \quad \rho = \bar{c}\rho_s + (1 - \bar{c})\rho_w$$

where $\bar{c}$ is total volumetric concentration, written as

$$15. \quad \bar{c} = \sum_{k=1}^{N} c_k$$

The transport equation for a certain fraction in conservative form reads

$$16. \quad \frac{\partial}{\partial t}\int_\Omega c_j \mathrm{d}\Omega + \int_S c_j \vec{v}_{z,j} \,.\, \vec{n} \mathrm{d}S = \int_S (\Gamma \nabla c_j) \,.\, \vec{n} \mathrm{d}S$$

where $\vec{v}_{z,j}$ is velocity vector of the sediment particle size j. The first term gives the rate of change of the concentration of a fraction, the second term represents the transport of that fraction owing to advection. The diffusive transport (caused by turbulence) is given on the right-hand side. The diffusion coefficient Γ is related to the eddy viscosity with the Schmidt–Prandtl number σ

$$17. \quad \Gamma = \frac{v_e}{\sigma}$$

Generally this number is regarded as constant throughout the computational domain. Rodi (1993) and Uittenboogaard (1995) showed that in free turbulence, even in highly stratified conditions, $\sigma = 0{\cdot}6$ can be used. The mixture model approach is used. This implies that in the horizontal direction the particle velocity is equal to the mixture velocity as computed with the RANS equations. In the vertical direction a slip velocity between the fluid velocity and grain velocity is assumed due to gravity (settling of the particles). For a mono-sized mixture (only one particle diameter present) the slip velocity equals the settling velocity w_s of that size, which is a function of the concentration

$$18. \quad w_s = w_0(1-c)^a$$

where a is exponent of hindered settling function. For a multi-sized mixture it is more complicated. The different sizes have a mutual influence. It is shown in Mirza and Richardson (1979) and van Rhee (2002) that the vertical velocity $v_{z,j}$ of a particle of size D_j in a mixture of N different particle sizes reads

$$19. \quad v_{z,j} = w + \sum_{k=1}^{N} c_k v_{s,k} - v_{s,j}$$

where the slip velocity $v_{s,j}$ reads

$$20. \quad v_{s,j} = w_{0,j}(1-\bar{c})^{a_j - 1}$$

in which $w_{0,j}$ is the settling velocity of a single particle with diameter D_j and a_j is the hindered settling exponent of that particle size. The value of this exponent varies between 2·6 and 5, depending on the particle size (Richardson and Zaki, 1954; Rowe, 1987).

3.4 Boundary conditions

Boundary conditions must be prescribed to solve the system of equations at the water surface, the sandbed and the left and right boundary of the computational domain.

3.4.1 Horizontal and vertical velocity

At the water surface the vertical velocity is zero and for the horizontal velocity the shear stress is zero at the water surface. At the sand bed the normal velocity is zero. For the velocity parallel to the wall a so-called wall function approach is used (Versteeg, 1995). This method assumes a logarithmic velocity profile at the wall and the relation between the shear stress and the velocity at a certain distance from the wall is according to the 'law of the wall'

$$21. \quad \tau_b = \frac{\rho u_Y^2}{\left(\frac{1}{k}\ln\left(\frac{32\,Y}{k_s}\right)\right)^2}$$

where τ_b is shear stress on bottom cell, Y is distance to the wall (bed) of velocity gridpoint, u_Y is velocity in the gridpoint close to the wall, κ is von Kármàn constant and k_s is roughness height according to Nikuradse. At the inlet zone (where the mixture leaves the hopper) the vertical velocity is prescribed as a function of time and the horizontal velocity is zero.

3.4.2 Bed boundary condition

At the water surface the sediment flux is zero, since no sediment can leave the domain at this location. An important condition is prescribed at the sand bed surface, which determines sedimentation or erosion at this location. The sedimentation velocity v_{sed}, defined as the vertical velocity of the seabed (interface between settled sediment and water/mixture above the bed), reads

$$22. \quad v_{sed} = \frac{S - E}{\rho_s(1 - n_0 - \bar{c}_b)}$$

where S is sedimentation flux, E is erosion or pick-up flux and $\bar{c}_b$ is near bed concentration. The sedimentation flux for a mono-sized mixture reads

$$23. \quad S = \rho_s w_s c_b$$

For a multi-sized mixture the value of S reads

$$24. \quad S = \rho_s \sum_{j=1}^{N} v_{z,j} c_{b,j}$$

where $v_{z,j}$ is computed using Equation 19. The pick-up flux E is more difficult to determine. One could use existing pick-up functions (Cao, 1997; van Rijn, 1984), but these functions are empirical and calibrated on experiments with relatively low values of concentration and flow velocity above the bed. It was shown by van Rhee (2010) and van Rhee and Talmon (2000) that application of the existing pick-up functions for the situations typically encountered in dredging (high concentration and flow velocities), leads to overestimation of sediment pick-up.

Special experiments were performed to determine pick-up at high values of the concentration and bed shear stress (van Rhee, 2002; van Rhee and Talmon, 2000). The sedimentation velocity was written as the product of the sedimentation

velocity for stagnant flow conditions and a reduction factor

$$v_{sed} = \frac{S}{(1 - n_0 - c_b)\rho_s} R(\theta) \quad (25)$$

The reduction factor $R(\theta)$ is a simple relation based on experiments (van Rhee, 2002).

$$R(\theta) = \begin{cases} 1 - \dfrac{\theta}{\theta_0} & \text{if } \theta < \theta_0 \\ 0 & \text{if } \theta \geq \theta_0 \end{cases} \quad (26)$$

The reduction factor is a function of the Shields parameter θ, which is defined as

$$\theta = \frac{u_*^2}{\Delta g D_{50}} \quad (27)$$

where θ_0 is an empirical constant with a value between 4 and 5, u_* is the friction velocity, by definition $\sqrt{\tau_b/\rho}, \Delta = (\rho_s - \rho_w)/\rho_w$, the specific density of the particles and τ_b is the bed shear stress. The limitation of this approach is that it can only be applied for flows where sedimentation is dominant and no erosion occurs. A pick-up function suitable for high flow velocity and steep slope angles was presented in van Rhee (2010). This function was based on the pick-up function of van Rijn (1984). Preliminary calculations (van Rhee, 2013) showed that the pick-up of this function was too large for the situation for high concentration and value of the Shields parameters between 1 and 5. Therefore the empirical function as presented in van Rhee (2013) and van Rhee and Talmon (2010) will be extended to include the effect of steep slopes and high flow velocity. The pick-up function used in van Rhee (2013) reads

$$\Phi_p = 0{\cdot}0025(D_* - 2{\cdot}4)^{0{\cdot}3} \frac{1 - n_0 - C_b}{1 - n_0} \theta \quad (28)$$

where $\Phi p = E/(\rho_s u_s)$ is dimensionless pick-up, $u_s = \sqrt{\vec{g}\Delta D_{50}}$ and D^* is dimensionless particle size defined as $D^* = D_{50}\sqrt[3]{\frac{\Delta \vec{g}}{\nu^2}}$. Following van Rhee (2010), this empirical function is now written as

$$\Phi_p = A \frac{\theta}{\theta'_{cr}} R_c \quad (29)$$

where A is constant, $R_c = (1 - n_0 - c_b)/(1 - n_0)$ is reduction factor for near bed concentration. The critical Shields parameter including the effect of high-speed erosion reads (van Rhee, 2010)

$$\theta'_{cr} = \theta_{cr}\left(\frac{\sin(\varphi - \alpha)}{\sin\varphi} + v_e \frac{\Delta n}{k_1(1 - n_0)\Delta}\right) = \theta_{cr}(R_\alpha + A_1 v_e) \quad (30)$$

where R_α is effect of slope on critical Shields value, α is slope angle and $A_1 v_e$ is effect of high-speed erosion on Shields value. This modified critical Shields parameter has the advantage that it yields the active wall velocity for slopes with angles larger than the internal friction angle (van Rhee, 2010). Using Equation 29 and Equation 30, the erosion velocity can now be computed with

$$v_e = \frac{A u_s \dfrac{\theta R_c}{\theta_{cr}(R_\alpha + A_1 v_e)} - w_s c_b \cos\alpha}{1 - n_0 - c_b} \quad (31)$$

Note that the erosion velocity v_e also appears at the right-hand side of the equation. The equation can, however, be rewritten to an explicit expression for v_e. The erosion velocity can also become negative (i.e. sedimentation) when the settling flux (i.e. last term in numerator of Equation 31) becomes larger than the pick-up flux.

The RANS equations are solved using a finite volume method on a rectangular grid. A pressure correction method was used to solve the hydrodynamic pressure in the momentum equations. Near the bed a cut-cell technique was used to facilitate relocation of the bed boundary resulting from erosion or sedimentation.

4. Simulation of the breaching process

4.1 Model set-up

The model is applied on a sand bed with an initial slope angle of 1:4 (14°) with a total height of 14 m (from $x = 60$ m to $x = 115$ m). Near the toe a steep section of 4 m height with a slope angle of 4:1 (76°) is created by removing sand at the location of the toe. The hatched line shows the original slope. Two different sand types are simulated. A mono-sized sand type with a $D_{50} = 120$ μm and a multi-sized sand with a $D_{15} = 120$ μm and $D_{50} = 300$ μm with an initial porosity $n_0 = 0{\cdot}4$. Hence the difference between the two situations is the median particle size as the initial geometry and permeability of the two situations are equal.

4.2 Analysis of the results

Figure 5 shows the evolution of the slope for the two different situations. Figure 5(a) shows the slope development for fine sand. The active wall height increases from 4 m to almost 6 m during the simulation. The breaching process is clearly unstable. After some time (at $t = 9600$ s) the active slope reaches the top of the slope. Then the active slope height decreases with time but the failure process continues until the toe of the active wall reaches the sand surface.

Figure 5(b) shows the simulation of the coarser sand. Although the active wall velocity is the same as in the upper panel, the sand settles with a larger (21°) slope angle compared with the initial slope. This indicates a stable breaching process. The initial disturbance diminishes after some time.

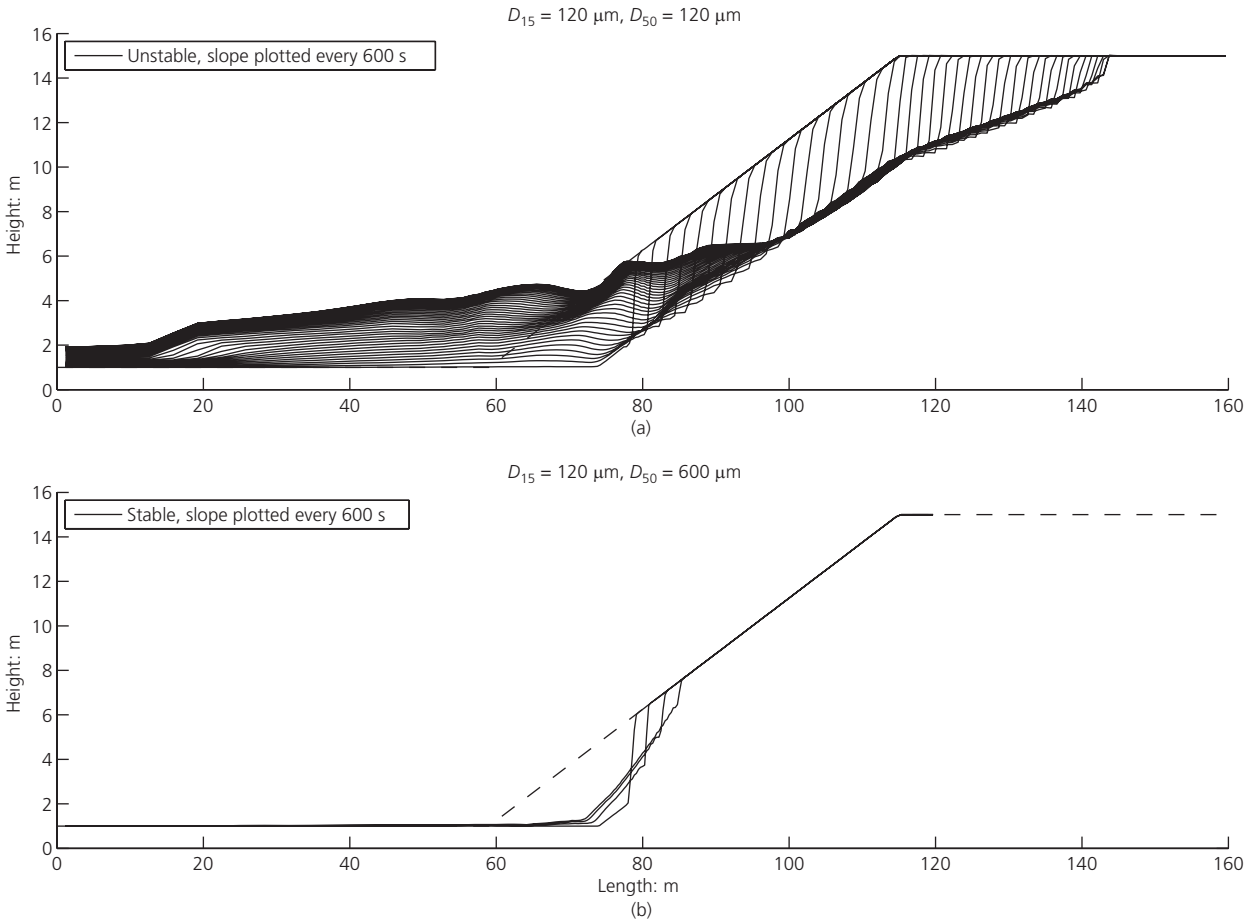

Figure 5. 2DV simulations of the breaching process for two different sands

Although the model is capable of simulating a breaching process and gives a first indication of whether a slope is susceptible to failure due to unstable breaching, the model is not yet suitable for design purposes. Validation with (large-scale) tests is still needed because the erosion function was not calibrated for large active wall heights, as can be observed in practice.

Furthermore, the current model is two-dimensional and it can be expected that the actual process will be three-dimensional. When a slope is eroded by a density current is can be expected that the erosion velocity will not be exactly equal over the width of the flow, for instance owing to slightly different soil properties. Therefore the height of the density current will vary over width. Where the height of the density current is larger, the flow velocity will also be larger compared with areas with smaller depth. Since the erosion velocity will increase with flow velocity, deeper areas will erode faster. Hence the flow will concentrate in deeper areas. A non-uniform distribution of the erosion velocity over width will not diminish but will be enlarged.

5. Conclusions

The unstable breaching process can result in failure of densely packed slopes. A simple stability criterion provides a first indication of whether a slope is susceptible to unstable breaching. The breaching process can be simulated using a 2DV mixture flow model using a boundary condition that includes the effect of breaching. Validation of the model is, however, still needed.

REFERENCES

Breusers HNC (1974) Suction of sand. *Bulletin of International Society of Engineering Geolology* **10**: 65–66.

Breusers HNC (1977) Hydraulic excavation in sand. *Proceedings of the International Course on Modern Dredging: Development in Techniques to Achieve Optimum Project*

Realisation. Post Graduate Courses in Civil Engineering, Technological University Delft and Royal Institute of Engineers, The Hague, the Netherlands.

Cao Z (1997) Turbulent bursting-based sediment entrainment function. *Journal of Hydraulic Engineering, ASCE* **123(3)**: 233–236.

de Jager RR, Mathijssen FAJM, Molenkamp F and Nooy van der Kolff AH (2008) Static liquefaction analysis using simplified modified state parameter approach for dredged sludge Depot Hollandsch Diep. *Proceedings of the 12th International Conference of International Association for Computer Methods and Advances in Geomechanics (IACMAG)* pp. 4748–4756, Goa, India.

den Adel H (1987) *Heranalyse doorlatendheidsmetingen door middel van de Forchheimer relatie*. GeoDelft, Deltares, Delft, the Netherlands, Technical report no. CO-272550/56 (in Dutch).

Groot M, van der Ruyt M, Mastbergen D and van der Ham G (2009) Bresvloeiing in zand. *Geotechniek* (in Dutch), nr. 3, pp. 35–39, Educom.

Koning JD (1970) Neue Erkenntnisse beim Gewinnen und Transport von Sand im Spülproject Venserpolder. In *Bauen im Ausland*. Verein Deutscher Ingenieure, Hamburg, Germany (in German).

Mastbergen DR and van den Berg V (2003) Breaching in fine sands and the generation of sustained turbidity currents in submarine canyons. *Sedimentology* **50(4)**: 625–637.

Mastbergen DR and Winterwerp JC (1988) On the construction of sand fill dams. Part 1: hydraulic aspects. In *Modelling Soil Water Structure Interaction*. (Kolkman P A, Lindenberg J and Pilarczyk K W (eds)). Balkema, Rotterdam, the Netherlands.

Meijer KL and van Os AG (1976) Pore pressures near moving underwater slope. *Journal of the Geotechnical Engineering Division, ASCE* **102(GT4)**: 361–372.

Mirza S and Richardson JF (1979) Sedimentation of suspensions of particles of two or more sizes. *Chemical Engineeirng Science* **34(4)**: 447–454.

Richardson JF and Zaki WN (1954) Sedimentation and fluidization: I. *Transacations of the Institute of Chemical Engineers* **32(35)**: 112.

Rodi W (1993) *Turbulence Models and their Application in Hydraulics: A State of the Art Review*, 3rd edn. IAHR Balkema, Delft, the Netherlands

Rowe PN (1987) A convenient empirical equation for estimation of the Richardson–Zaki exponent. *Chemical Engeering Science* **42(11)**: 2795–2796.

Torrey VH (1995) Flow slides in Mississippi river banks. In *River, Coastal and Shoreline Protection-erosion Control. Using Riprap and Armourstone* (Thorne CS, Abt SR, Barendt BJ, Maynard ST and Pilarczyk KW (eds)). Wiley, Chichester, UK, pp. 361–377.

Uittenboogaard RE (1995) *The Importance of Internal Waves for Mixing in a Stratified Estuarine Tidal Flow*. PhD thesis, Delft University of Technology, the Netherlands.

van Rhee C (2002) *On the Sedimentation Process in a Trailing Suction Hopper Dredge*. PhD thesis, Delft University of Technology, the Netherlands.

van Rhee C (2010) Sediment entrainment at high flow velocity. *Journal of Hydraulic. Engineering, ASCE* **136(9)**: 572–582.

van Rhee C (2013) Two dimensional simulation of sedimentation and erosion of sand. *Proceedings of the 16th International Conference on Transport and Sedimentation of solid particles, Rostock, Germany*, pp. 197–204.

van Rhee C and Bezuijen A (1998) The breaching of sand investigated in large-scale model tests. In *Coastal Engineering 1998* (Edge BL (ed.)). American Society of Civil Engineers, Reston, VA, USA, vol. 3 pp. 2509–2519.

van Rhee C and Talmon AM (2000) Entrainment of sediment (or reduction of sedimentation) at high concentration. *Proceedings of the 10th International Symposion on Transport and Sedimentation of Solid Particles, Wroclav, Poland*, pp. 251–262.

van Rhee C and Talmon A (2010) Sedimentation and erosion of sediment at high solids concentration. *Proceedings of Hydrotransport 18*, pp. 211–222, BHR Group, Bedford, UK.

van Rijn LC (1984) Sediment pick-up functions. *Journal of Hydraulic Engineering, ASCE* **110(10)**: 1494–1502.

Versteeg HK (1995) *An Introduction to Computational Fluid Dynamics; the Finite Volume Method*. Longman Scientific and Technical, Harlow, UK.

Vlasblom WJ (2003) Lecture notes course WB3413 dredging processes. *The Breaching Process*, Delft University of Technology, Delft, the Netherlands.

You Y, Flemings P and Mohring D (2012) Dynamics of dilative slope failure. *Geology* **40(7)**: 663–666.